IJMP

Original Article

Monte Carlo Study of the Effect of Backscatter Materail Thickness on 99mTc Source Response in Single Photon Emission Computed Tomography

Jalil Pirayesh Islamian [1], Mohammad Taghi Bahreyni Toossi [2]*, Mahdi Momennezhad [3],
Seyyed Rasool Zakavi [3], Ramin Sadeghi [3]

Abstract

Introduction
SPECT projections are contaminated by scatter radiation, resulting in reduced image contrast and quantitative errors. Backscatter constitutes a major part of the scatter contamination in lower energy windows. The current study is an evaluation of the effect of backscatter material on FWHM and image quality investigated by Monte Carlo simulation.

Materials and Methods
SIMIND program was used for simulation of a Siemen's dual-head variable angle scintillation gamma camera. Planar and SPECT scanning of a ^{99m}Tc source and a Jaszczak phantom for varying thicknesses of Perspex slabs, as a backscatter media, were analyzed using the photopeak and scatter windows. Simulated planar images and reconstructed tomographic images were evaluated qualitatively, by two nuclear medicine specialists, and quantitatively, by Structural Similarity (SSIM) Index.

Results
In the ^{99m}Tc photopeak window, no significant change in total counts due to backscatter material was measured. In the scatter windows, scattering was overestimated compared with a simulated backscatter free SPECT system. For instance, at a thickness of 10 cm, total counts of a ^{99m}Tc source detected in the 72 keV windows eventually doubled with increasing backscatter material, compared with the situation without backscatter material. The backscatter contribution plateaued when more than 7 cm of scatter material was placed but there were optimized results for a backscatter thickness of 4.5 cm. Better image quality for the thickness was confirmed by the results of eye interpretation and also by SSIM algorithm.

Conclusion
Backscatter should be taken into account, particularly in model-based scatter correction methods in SPECT for an accurate simulation system optimization.

Keywords: Backscatter Media, Image Quality, Resolution, SIMIND Monte Carlo, Single Photon Emission Computed Tomography

1- *Medical Physics Department, Faculty of Medicine, Tabriz University of Medical Sciences, Tabriz, Iran.*
2- *Medical Physics Research Center, Medical Physics Department, Mashhad University of Medical Sciences, Mashhad, Iran.*
   Corresponding author: Tel: 0511-8828576; Fax: 0511-8002320; Email: bahreynimt@mums.ac.ir
3- *Nuclear Medicine Department, Imam Reza Hospital, Mashhad University of Medical Sciences, Mashhad, Iran.*

1. Introduction

Scattering has a degrading role in nuclear medicine imaging. Photon interactions in the patient body, media between the patient and gamma camera, and also the camera structures contribute to the scatter. On the other hand, the gamma cameras commonly used in nuclear medicine have limited energy resolution. To detect sufficient photons, a broad photopeak window is used, which permits the detection of scattered photons. In several situations, scatter can account for more than half of all the counts detected in the photopeak window [1], and thus causes degradation in image contrast and quantitative accuracy. Therefore, it is necessary to consider the contribution of each of the structures to the scatter ratios. The structures at the back of scintillation crystal such as light guides and photomultiplier tubes (PMTs) contribute in backscattering, especially when high energy radionuclides, e.g., ^{131}I are used. Modeling the backscatter of photons behind the crystal is a difficult task because of the complex geometry of light guides and PMTs, for some applications, especially for radionuclides that emit photons of energies higher than the principal energy. Scattering of these photons back into the crystal can cause degradation of the image quality. Figure 1 shows a graph of the ^{131}I simulation when backscattering has been included [2].
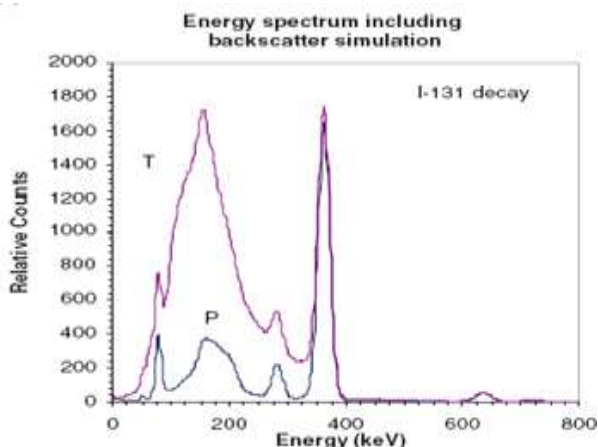

Figure 1. Energy spectrum from the ^{131}I simulation with backscattering behind the scintillation NaI(Tl) crystal. The events from the primary photons (P) and the total number of events (T) are shown separately. The y axis is scaled by the photon events [2].

To include this in the model, an equivalent layer of a backscattering material can be defined that allows scattering back into the crystal. The difficult task is then to determine the thickness and composition of the layer so that the same scattering conditioning as in the light-guide and PMTs can be achieved [3].
There are some scatter correction methods for compensation of the above-mentioned matter. The most general scatter correction methods proposed are based on Monte Carlo simulation [4,5] or on analytical photon-transport equations including Klein-Nishina (K-N) equations [6-8]. These methods can readily handle non-uniform attenuating media. However, generation of the transition matrix has to be repeated for every SPECT study which makes excessive demands on the processing time and memory consumption, especially when photon cross-talk between slices is being modeled (fully 3D reconstruction). In ^{99m}Tc/^{153}Gd combined Emission-Transmission CT, which allows accurate attenuation and scatter correction, down-scatter of ^{99m}Tc photons hampers the reconstruction of the transmission map [9-11]. For model-based down-scatter correction, it is therefore mandatory to know the scatter response of ^{99m}Tc (140 keV) in the ^{201}Tl (72 keV) and ^{153}Gd (100 keV) photopeak windows [12,13]. One class of scatter correction methods incorporates the scatter models in iterative reconstruction and also pre- or past-reconstruction filtering [14]. This gives a better contrast-to-noise ratio of small cold lesions than subtraction-based methods. In addition, knowledge of the scatter response can be used to simulate SPECT in a realistic way [7,15]. The response of a source in an arbitrary object can also be approximated from a series of responses of line sources measured behind slabs of various thicknesses (slab-derived scatter compensation as described in [16] and [17]). These models are known to give highly quantitative images when used in iterative scatter correction [18]. Slab-derived scatter models can be regarded as a practical

alternative to the time-consuming, but more general MC or K-N-based methods, but such models do not incorporate the detection of photons scattering via material behind the source. The purpose of this study was to investigate the effect of scatter material behind the detector, by SIMIND Monte Carlo simulation [19], on the ^{99m}Tc photopeak and scatter windows by FWHM and image quality analysis: i) visual inspection and ii) using Structural Similarity (SSIM) index, a method for measuring the similarity between two images [20]. The SSIM index is a full reference metric, in other words, measuring image quality is based on an initial uncompressed or distortion-free image as the reference. SSIM is designed to improve traditional methods such as peak signal-to-noise ratio (PSNR) and mean squared error (MSE), which have proved to be inconsistent with human eye perception [21].

2. Materials and Methods

2.1. Imaging system

A dual-headed variable angle scintillation gamma camera (Siemens Medical Solutions, Erlangen, Germany) equipped with two rectangular detectors with a field of view (FOV) of 53.3×38.7 cm^2 and 9.5-mm-thick NaI (Tl) crystals, installed in Nuclear Medicine Department of Imam Reza Hospital of Mashhad University of Medical Sciences Mashhad, Iran, as illustrated in Figure 2, was used in this study and also for the Monte Carlo simulations. The camera consists of two removable Low Energy High Resolution (LEHR) collimators. The parameters of LEHR collimator, used for low-energy sources such as ^{99m}Tc, for experiment and simulation are shown in Table 1. The NaI (Tl) crystal specifications are as follows: Planar, 9.5 mm in thickness, 59.1×44.5 cm^2 in area, light yield 40k photons/MeV, and a peak emission spectrum at 415 nm [22,23]. Emitted scintillation light photons were collected by a matrix composed of 59 PMT, 53 with a diameter of 7.6 cm and 6 with 5.1 cm. The photocathode is of the bialkali type with a quantum efficiency of approximately 30% for

the wavelength of maximum NaI (Tl) emission [24]. A light guide ensured maximum collection of light and optical grease results in good optical coupling between the scintillating crystal and PMTs.

Figure 2. A dual-headed variable angle scintillation gamma camera, Siemens Medical Solutions, Erlangen, Germany, was used in the simulation study.

2.2. Monte Carlo Simulation

SIMIND Monte Carlo program was used for simulating the camera [25,26]. The simulated system verification was done by confirming exact coincidence of the systems performance parameters such as energy spectrum, spatial resolution, and energy resolution (for details refer to Bahreyni Toossi et al. [26]). In order to investigate the influence of backscatter material, a Pyrex slab as a backscatter media, composed of K, Si, Al, Na, O, and B with percentage weights of 0.3, 37.7, 1.2, 2.8, 54, and 4%, respectively, was substituted and simulated [3]. The dimensions of the square Perspex slab was 44.5×59.1 cm^2 with thicknesses from 0.5 to 10 cm and a density of 1.185 g/cm^3 [3].

Increases in total counts due to backscatter material are calculated as a percentage of the total counts in the situation where no backscatter material was present. Hence, no increase gives 0%, and 100% means that the

total counts have been doubled due to backscatter material. Furthermore, the Full Widths at Half Maximum (FWHM) was calculated.

2.3. Phantoms

A ^{99m}Tc point source, a line source, and an acrylic cylindrical Jaszczak Deluxe phantom [27,28] were used both for experiment and simulation studies. The ^{99m}Tc point and line sources have been considered to have an activity of 37 MBq, with an isotropic source emitting 140 keV photons. To obtain the output spectra of the simulated gamma camera a ^{99m}Tc point source was simulated for the following geometries and activities: i) 3.7 MBq, without collimator, positioned at 0, 10, 15, 20, and 25 cm from the detector surface, ii) 37 MBq, with collimator and at the same distances as mentioned, and iii) 37 MBq, with collimator, and 1-10 cm slabs of Pyrex, as backscatter material.

Moreover, the acrylic cylindrical Jaszczak Deluxe phantom, with spherical inserts measuring 9.5, 12.7, 15.9, 19.1, 25.4, and 31.0 mm in diameter and insert of rods measuring 4.8, 6.4, 7.9, 9.5, 11.1, and 12.7 mm diameter, was filled with water and 370 MBq activity of ^{99m}Tc. As the SIMIND simulated SPECT projections are noise-free, for realization, we added noise according to the administered dose.

2.4. Image Acquisition

In this work, we have studied i) the energy resolution, ii) the spatial resolution, and iii) the image contrast as function of 20 different backscatter thickness material, ranging from 0.5 to 10 cm, according to the published quality control tests [29-35]. A 130-151 keV energy window was centered on the ^{99m}Tc photopeak [34]. Spatial and energy resolutions were determined by placing the point source at the center of the FOV, at 10 and 25 cm from lower collimator surface, respectively, for both simulation and experiment. An energy pulse-height distribution was acquired for 10^7 photons/projection with various thicknesses of the backscatter media. A study of the SPECT reconstructed spatial resolution was also carried out both experimentally and by

SIMIND simulation with the line source. SPECT projections along the axis of rotation were also acquired from the Jaszczak Deluxe phantom [28], which was positioned 15 cm from the collimator surface. Spatial resolution was obtained from viewing the smallest visible and recognizable rods. The images were reconstructed in matrices of 128×128 pixels, with a pixel size of 0.39 mm. The images were reconstructed and processed by Filtered Back Projection (FBP) reconstruction using a ramp filter combined with a Butterworth filter of order 5 and cut-off frequency 0.45 cycles/cm.

2.5. Image Evaluation

The qualities of images were evaluated, qualitatively by two nuclear medicine specialists, and quantitatively by SSIM index algorithm. The SSIM metric was calculated on various windows of an image. The measure between two windows x and y of common size N×N was:

$$SSIM(x; y) = \frac{(2\mu_x\mu_y + C_1)(2\sigma_{xy} + C_2)}{(\mu_x^2 + \mu_y^2 + C_1)(\sigma_x^2 + \sigma_y^2 + C_2)}$$

Where, μ_x and μ_y are the average of x and y and σ_x^2 and σ_y^2 are the variance of x and y, respectively. σ_{xy} is the covariance of x and y. $C1 = (k_1L)^2$, $C_2 = (k_2L)^2$ are two variables to stabilize the division with weak denominator. L is the dynamic range of the pixel values (L = 255 for 8 bits/pixel gray scale images) and finally, $k_1 = 0.01$ and $k_2 = 0.03$ by default.

Approximately, μ_x and σ_x can be viewed as estimates of the luminance and contrast of x, and σ_{xy} measures the tendency of x and y to vary together, thus an indication of structural similarity [21].
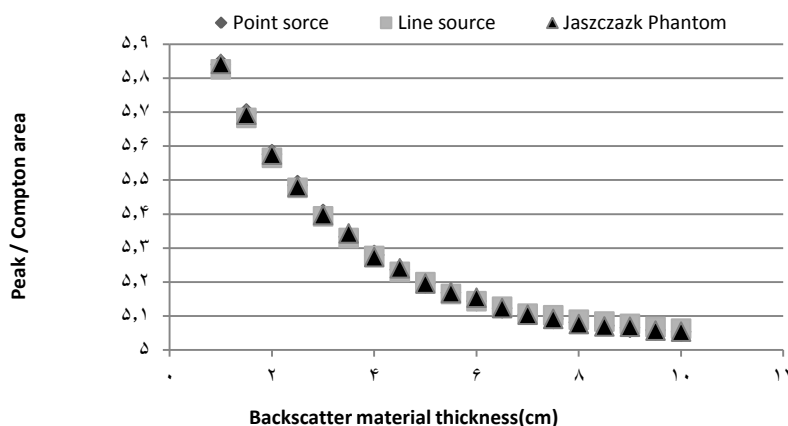
3. Results

We simulated a dual-headed variable angle scintillation gamma camera and related backscatter structures, equaled as a slab of Pyrex, with SIMIND Monte Carlo program.

Figure 3 (a and b) shows the obtained scatter curves of the effect of backscatter material thickness on the Peak to Compton and also Compton Area in the ^{99m}Tc energy spectrum for simulation results from the SPECTs of the
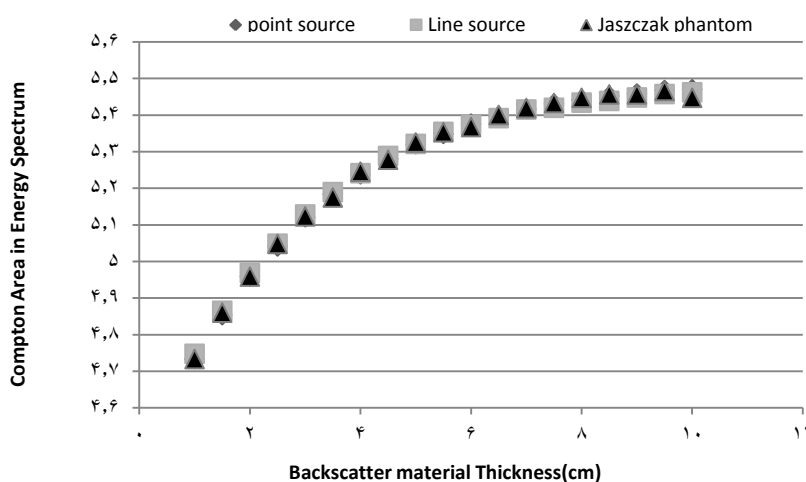
phantoms with different thicknesses of Pyrex, as a backscatter material, by SIMNID Monte Carlo program. For instance, at a thickness of 10 cm, total counts of a ^{99m}Tc source detected in the 72 keV windows eventually doubled with increasing backscatter material, compared with the situation without backscatter material.

The backscatter contribution plateaued when more than 7 cm of scatter material was placed. There was also some progressive increasing in FWHM for increasing the backscatter material thickness, especially from 1 to 6 cm thickness, on the related energy spectrums.

(a)

(b)

Figure 3. Scatter curve from the effect of backscatter material thickness on the Peak to Compton Area (a) and Compton area (b) in energy spectrum. The results for simulation of a point source scanning, a line source, and a Jaszczak phantom with different thicknesses of Pyrex, as a backscatter material, by SIMNID monte carlo program.

For the reconstructed SPECT images of the Jaszczak phantom, the smallest observed cold sphere was 12.7 mm in diameter with all of the Pyrex thicknesses. The results of the images quality by visual inspection apparently showed

no differences in resolutions and contrasts of the images but there were some differences in the image quality parameters, especially SSIM indexes.

A strong increase in total counts with increasing backscatter material was measured, except for the photopeak window. The increase in counts due to backscatter material was steeped in the first few centimeters of backscatter material, 1-6 cm, but plateaus eventually, at about 7-10 cm.

4. Discussion

Scattering have a degrading role on image contrast and quantitative accuracy of SPECT imaging and numerous studies have been dedicated for eliminating and/or correcting its effect [36]. The goal of this study was to investigate the influence of backscatter material on ^{99m}Tc source responses in photopeak and scatter windows. De Vries et al. have determined an equal thickness of a layer from Pyrex, composed of K, Si, Al, Na, O, and B with percentage weights of 0.3, 37.7, 1.2, 2.8, 54, and 4%, respectively, which produced the same scattering conditioning as in the light-guide and PMTs [3]. They used a thickness of 6.6 cm and a density of 66% of that of Pyrex as an equal effective backscatter compartment for energy range of ^{131}-I. On the other hand, there are several parameters of SPECT acquisition which affect backscatter detection, such as energy resolution of the system, density of the interacting medium, and width and location of the energy windows.

Using the theory and considerations presented in Figures 3 and 4, one can explain the obtained results. These considerations may be useful for predicting trends in other experimental situations. One of the most important features of the results is the plateau effect. At small backscatter thicknesses, the probability that a photon backscatters is small because of the limited scatter angles. Increasing the backscatter thickness allows more photons to backscatter. However, photons scattered at large backscatter depths are less likely to be detected because they are more attenuated. At the same point, addition of extra material ceases to affect the yield anymore because the thick layer of backscatter material strongly attenuates the photon flux. We have shown that 4.5 cm of backscatter material accounts for approximately the best realized counts with some steeper slop for the thickness up to 4.5 cm. Therefore, a first order method for including backscatter in the slab-derived scatter model may be to add a 4.5 cm backscatter material to the slab measurements. The results of scattering in energy spectrum for SPECT scanning of a ^{99m}Tc point source, a ^{99m}Tc line source, and also a Jaszczack phantom coincide exactly and therefore, confirm the findings.

Figure 3 shows energy spectra of a ^{99m}Tc point source in a scattering medium with and without backscatter material, generated with the SIMIND Monte Carlo code [37]. SIMIND was validated by its author using scatter-to-primary ratios, scatter responses, and energy spectra. At high energies, the spectra in both scatter situations are identical. At energies below maximum E_f, backscattered photons increase the number of detected photons compared with the scatter situation without backscatter material. In reality, this spectrum is always blurred by typically 10%, but these simulations were done with perfect resolution in order to link the calculations to the spectra. The possibility that a photon backscatters with maximum $\theta_i = 180^0$ or minimum energy loss $\sum \theta_i = 90°$ is small. For the latter case, all scatter angles must be unidirectional, all must be equal to $\theta_i = \frac{1}{n}\theta_{total}$, and the scatter events must lie in one plane. The sum of scatter angles will most probably be between the two extremes (Figure 4).

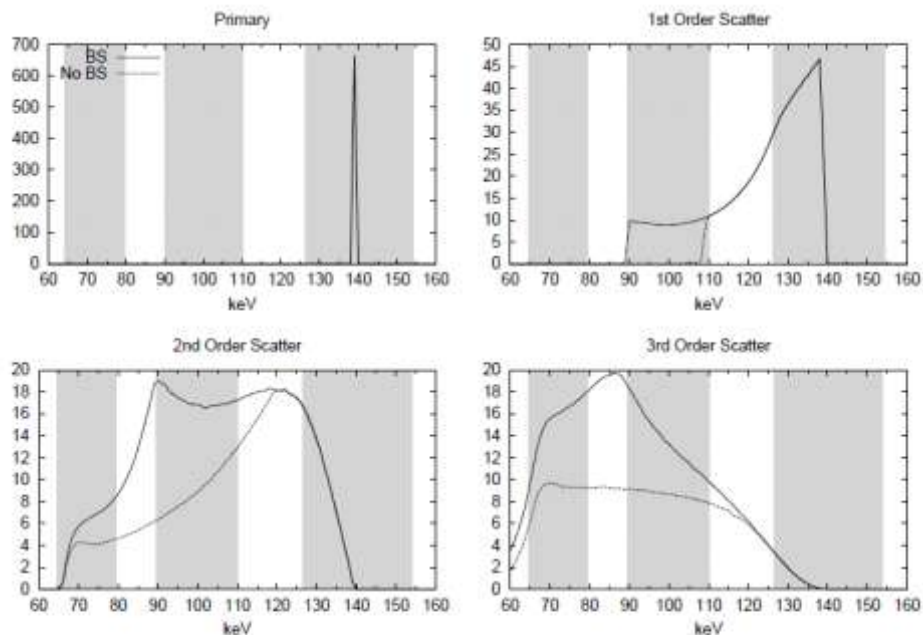Figure 4. Monte Carlo generated energy spectra of primary, first order, second order, and third order scattered ^{99m}Tc photons (E_0=140KeV) in a situation with backscatter material (BS) and without (No BS) using ideal detector resolution. Position of energy windows is illustrated by the shaded boxes. Left box: 72±10% keV, centre box: 100±10% keV, right box: 140±10% keV [37].

Using the simple analytical descriptions of photon transport, one can predict to a certain extent the influence that backscattered photons will have on the responses. Figure 3 shows that backscattered ^{99m}Tc photons cannot be detected in the photopeak window (126-154 keV) unless they have scattered at least three times. Even then, they are very unlikely to be detected in the photopeak window. This is because of the limited allowed scatter angles for detection (only few photons can backscatter in $\theta_{total} = 90°$, have equally distributed scatter angles, have all scatter events in one plane, and satisfy the unidirectional demand). Increasing the scatter angles of these photons brings down to 125 keV and makes their final energy fall outside the energy window. The energies of the majority of backscattered photons correspond with the energy settings of the scatter windows; hence the responses in these windows are likely to be influenced by backscatter material. For down-scatter windows, the maximum energy loss is important as well as the minimum energy loss of backscattered photons. For example, in the ^{99m}Tc scatter window, no first order scatter is

detected. Responses in these windows are dominated by multiple order scatters and thus they are broader than responses in the photopeak window. Therefore, our study has considered and acquired the results for third order scatter in the window. On the other hand, a recent study on Monte Carlo modeling of the back compartments of SPECT cameras for dual isotope simultaneous acquisition, have shown the manifest effect of the highest energy isotope detection in the imaging energy window of the second isotope and so on the simulation accuracy of high-energy isotopes [38]. Their results showed that an accurate description of the backscatter compartments is required for SPECT simulations of high-energy isotopes (above 300 keV) when the backscatter energy window is of interest.

5. Conclusion

SPECT has a lower resolution compared with most other 3D imaging modalities, but can image the perfusion and function at low costs if the scatter problem perfectly resolved. SPECT is widely used so lots of experiences in the last decades have been acquired concerning diagnosis and prognosis. Monte

Carlo simulations can be used to increase the speed of such studies. SIMIND Monte Carlo simulation of scatter in SPECT has tremendously been accelerated by stochastic Monte Carlo simulation methods combined with analytical simulation methods. Proper treatment of scatter may improve the accuracy and yield of the simulations.

References

1. Floyd CE, Jaszczak RJ, Coleman RE. Scatter detection in SPECT-imaging: dependence on source depth, energy, and energy window. Phys Med Biol 1988;33(9): 1075–1081.
2. Ljungberg M. Simulation Techniques and Phantoms. In:Wernick M, Aarsvold J, editors. Emission Thomography : The Fundamentals of PET and SPECT. New York: Elsevier Academic Press; 2004: 551-63.
3. De Vries DJ, Moore SC, Zimmerman RE, Mueller SP, Friedland B, Lanza RC. Development and validation of a Monte Carlo simulation of photon transport in an anger camera. IEEE Trans Med Imaging 1990;9(4):430-8.
4. Floyd CE , Jaszczak RJ, Greer KL, Coleman RE. Inverse Monte Carlo as a unified reconstruction algorithm for ECT. J Nucl Med 1986;27(10):1577–1585.
5. Ljungberg M. The SIMIND Monte Carlo program, In: Monte Carlo Calculations in Nuclear Medicine, M. Ljungberg and S. E. Strand and M. A. King eds, IOP Publishing, UK ; 1998:145–163.
6. Cao ZJ, Frey EC, Tsui BMW. A scatter model for parallel and converging beam SPECT based on the Klein-Nishina formula. IEEE Trans Nucl Sci 1994;41(4):1594–600.
7. Riauka TA, Gortel ZW. Photon Propagation and Detection in Single Photon Emission Computed Tomography - An Analytical Approach. Med Phys 1994;21(8):1311–21.
8. Walrand SH, van Elmbt LR, Pauwels S. Quantification in SPECT using an effective model of the scattering. Phys Med Biol. 1994;39(4):719-34.
9. Heller EN, DeMan P, Liu YH, Dione DP, Zubal IG, Wackers FT, Sinusas AJ. Extracardiac Activity Complicates Quantitative Cardiac SPECT Imaging Using a Simultaneous Transmission- Emission Approach. J Nucl Med 1997;38(12): 1882–1890.
10. Beekman FJ, Kamphuis C, Hutton BF, van Rijk PP. Half-Fan-Beam Collimators Combined With Scanning Point Sources For Simultaneous Emission Transmission Imaging. J Nucl Med 1998;39(11):1996 2003.
11. Tan P, Bailey DL, Meikle SR, Eberl S, Fulton RR, Hutton BF. A scanning line source for simultaneous emission and transmission measurements in SPECT. J Nucl Med 1993; 34(10): 1752– 1760.
12. Kadrmas DJ. Application of Reconstruction-Based Scatter Compensation to Single- and Dual-Isotope SPECT Imaging., Ph.D. thesis, The University of North Carolina at Chapel Hill, 1997.
13. Beekman FJ, Kamphuis C, Slijpen ETP, van Rijk PP. Model-Based Down-Scatter Correction of Attenuation Maps in Simultaneous Emission Transmission Imaging. J Nucl Med 1998;39:178.
14. Lyra M, Ploussi A. Filtering in SPECT Image Reconstruction. Int J Biomed Imaging. 2011;2011:1-14. doi:10.1155/2011/693795
15. Beekman FJ, Viergever MA. Fast SPECT Simulation Including Object Shape Dependent Scatter.IEEE . IEEE Trans Med Im 1995;14(2):271–282.
16. Beekman FJ, Eijkman EGJ, Viergever MA, Borm GF, Slijpen ETP. Object Shape Dependent PSF Model for SPECT imaging. IEEE Trans Nucl Sci 1993;40(1):31–39.
17. Frey EC, Tsui BMW. A Practical Method for Incorporating Scatter in a Projector-Back projector for Accurate Scatter Compensation in SPECT. IEEE Trans Nucl Sci 1993;40(4):1107–1116.
18. Beekman FJ, Kamphuis C, Viergever MA. Improved Quantitation in SPECT Imaging Using Fully 3D Iterative Spatially Variant Scatter Compensation. IEEE Trans Med Im 1996;15(4): 491–499.

19. Ljungberg M, Strand SE. A Monte Carlo program for the simulation of scintillation camera characteristics. Comp Meth Prog Biomed 1989;29:257-72.

20. Rouse DM, Hemami Sh S. Analyzing the Role of Visual Structure in the Recognition of Natural Image Content with Multi-Scale SSIM. Proccedings of SPIE Human Vision and Electronic Imaging XIII, San Jose, CA 2008: 1-14.

21. Wang Z, Simoncelli EP, Bovik AC. Multi-scale structural similarity for image quality assessment. Proccedings of 37th IEE Asilomar conference on signals, systems, and computers, Pacific Grove, CA 2003; 9-12.

22. Data sheet of Siemens E.CAM Dual Head gamma camera. 1992. p. 1-12.

23. Vittori F, Notaristefani F, Malatesta T. Crystals and light collection in Nuclear Medicine. Nucl Phys B 1999;78(1):616-21.

24. Motta D, Schnert S. Optical properties of bialkali photocathodes. Nucl Instr Meth Phys Res A 2005;539:217-35.

25. The SIMIND Monte Carlo Program. Available from: http://www. radfys.lu.se/simind. [cited in 2011].

26. Bahreyni Toossi MT, Islamian JP, Momennezhad M, Ljungberg M, Naseri SH. SIMIND Monte Carlo simulation of a single photon emission CT. J Med Phys 2010;35(1):42-7.

27. Data sheet of Flangeless Deluxe Jaszczak SPECT Phantom. Available from:http://www.spect.com/pub/Flangeless_Jaszczak_Phantom.doc.pdf. [cited in 2011].

28. Groch MW, Erwin WD. Single-photon emission computed tomography in the year 2001: Instrumentation and quality control. J Nucl Med Technol 2001; 29:9-15.

29. AAPM Report No 22. Rotating Scintillation camera SPECT acceptance testing and quality control. , American Institute of Physics,USA:1987.

30. National Electrical Manufacturers Association. Recommendations for implementing SPECT instrumentation quality control. J Nucl Med 2000;41:383-9.

31. National Electrical Manufacturers Association (NEMA).Performance Measurements of Scintillation Cameras. NEMA NU1-2001. Washington, USA; 2001.

32. Quality Control of Nuclear Medicine Instruments. Vienna, Austria:IAEA; 1991.

33. IPEM 86. Quality Control of Gamma Camera Systems. Institute of Physics and Engineering in Medicine, York, England: 2003.

34. Nuclear Medicine Resources Manual IAEA, Vienna, Austria: 2006.

35. Jarritt PH, Perkins AC, Woods SD. Audit of nuclear medicine scientific and technical standards. Nucl Med Commun 2004; 25:771-5.

36. Hutton BF, Buvat I, Beekman FJ.Review and current status of SPECT scatter correction. Phys Med Biol 2011; 56(14): 85–112.

37. Jong HWAM, Beekman FJ, Ljungberg M, van Rijk PP. The influence of backscatter material on 99mTc and 201Tl line source responses. Phys Med Biol 1999; 44(3): 665. doi:10.1088/0031-9155/44/3/003

38. Rault E, Staelens S, Van Holen R, De Beenhouwer J, Vandenberghe S. Accurate Monte Carlo modelling of the back compartments of SPECT cameras. Phys Med Biol 2011;56(1):87-104.